# A Multifrequency Superposition Methodology to Achieve High Efficiency and Targeted Power Distribution for a Multiload MCR WPT System

Fuxin Liu, *Senior Member, IEEE*, Yong Yang, Ze Ding, Xuling Chen, *Member, IEEE*, and Ralph M. Kennel, *Senior Member, IEEE*

***Abstract*—Magnetically coupled resonant (MCR) wireless power transfer (WPT) is one of the most promising WPT technologies for its remarkable capability of simultaneous noncontact power transfer for multiple independent loads. Nevertheless, diverse energy requirements of different loads and efficiency quota make it difficult to design and optimize the multiload system. In this paper, a novel driver configuration for the MCR WPT system with multiple loads is proposed, in which the transmitting resonant tank is driven synchronously by multiple inverters operating at multiple switching frequency and sharing a common dc voltage source, then a multifrequency superposition methodology is presented to achieve high efficiency and targeted power distribution. The dominant features of the methodology are listed as follows: 1) the multifrequency power components from multiple inverters can be simultaneously delivered to multiple loads through a single transmitter; 2) the receiving coils are elaborately designed at different resonant frequencies that correspond to the operating frequencies of multiple inverters to achieve targeted power transfer and high efficiency; 3) the resonant frequency of the transmitter can be modulated within the adjacent area of multiple operating frequencies, and the power distribution to meet the requirements of selective loads will be realized; and 4) the resonant frequencies of receivers can also be adjusted to effectively realize the power distribution. In this paper, a double-frequency MCR WPT system with two loads is comprehensively investigated as a representative example, and the studied methodology has been experimentally verified by two prototypes of the proposed circuit configurations.**

Manuscript received October 5, 2017; accepted December 5, 2017. Date of publication December 21, 2017; date of current version July 15, 2018. This work was supported in part by the National Natural Science Foundation of China under Grant 51505223, in part by the Natural Science Foundation of Jiangsu Province, China, under Grant BK20151471, in part by the Lite-on Research Program, and in part by Jiangsu Province University Outstanding Science and Technology Innovation Team Project. Recommended for publication by Associate Editor W.-H. Ki. *(Corresponding author: Fuxin Liu.)*

F. Liu, Y. Yang, and Z. Ding are with Jiangsu Key Laboratory of New Energy Generation and Power Conversion, College of Automation Engineering, Nanjing University of Aeronautics and Astronautics, Nanjing 210016, China (e-mail: liufuxin@nuaa.edu.cn; yangyong_nuaa@126.com; dize1995.dize.1995@qq.com).

X. Chen is with College of Mechanical and Electrical Engineering, Nanjing University of Aeronautics and Astronautics, Nanjing 210016, China (e-mail: chenxuling@nuaa.edu.cn).

R. M. Kennel is with the Department of Electrical and Computer Engineering, Technical University of Munich, Munich 80333, Germany (e-mail: ralph.kennel@tum.de).

Color versions of one or more of the figures in this paper are available online at http://ieeexplore.ieee.org.

Digital Object Identifier 10.1109/TPEL.2017.2784566

***Index Terms*—Magnetically coupled resonant (MCR), multifrequency, multiload, targeted power distribution, wireless power transfer (WPT).**

## I. Introduction

TO SATISFY increasing requirements of various charging applications, such as electric vehicles, smart home, portable electronic devices, and implantable devices [1]–[4], widespread attention has been paid to the research work of wireless power transfer (WPT) for its great convenience of being cordless and safety in wet and harsh environment compared with the traditional cable power transfer. In 2007, a 60-W bulb was successfully lighted up over a distance above 2 m by scientists in Massachusetts Institute of Technology, which is viewed as a landmark event of rapidly developing WPT technologies [5]. Currently, magnetically coupled inductive (MCI) and magnetically coupled resonant (MCR) are two mainstream WPT technologies, which employ near field to transfer the power based on electromagnetic induction principles [6]. Some MCI WPT cases have exhibited high power transmission efficiency, normally larger than 90% within the transmission distance of several centimeters [7]. However, the transmission distance is still constrained due to the large leakage inductance of the loosely coupled transformers. In contrast, MCR WPT can cover wider transmission range with high efficiency and high power under loosely coupled conditions [8]; thus, it has become a hotspot in the midrange WPT applications at present.

For MCR WPT technology, simultaneous delivering power to multiple loads is a unique and attractive advantage. However, there are still numerous challenging issues of the operation of multiload MCR WPT systems, among which, high efficiency and power distribution are two important issues and have been gradually taken into consideration. Differed from single-load systems [9]–[12], the transmission characteristics of multiload systems are significantly affected by multiple loads and intricate couplings among transmitter and multiple receivers, which exhibit more complicated for the theoretical analysis and parameters design [13], [14]. Nowadays, some practical techniques based on single-frequency power transfer have been put forward to settle relevant issues. In [15], the resonant frequencies of multiple receivers are commonly designed at the operating frequency for maximum efficiency under specific loads, but the

condition for maximum efficiency does not necessarily guarantee maximum power transfer. To maximize the amount of power transfer, the resonant frequency of the transmitter need to be tuned to the same resonant frequency of receivers. However, the power distribution to the specific loads cannot be adjustable in this system. Yin *et al.* [16] present a method of cascading converters at the receiving sides to modulate equivalent load resistances for power distribution. The defect is that the system efficiency will fluctuate with the variation of equivalent load resistances and be difficult to maintain at high levels in some special operation points. Fu *et al*. [17] discuss the existence of optimal loads to achieve maximum efficiency for a general single-transmitter multireceiver system under a fixed operating frequency. Compared with the unified receiving resonant frequency mentioned above, different resonant frequencies of receivers are designed in [18]. One of multiple loads can obtain high power and high efficiency through adjusting the operating frequency to its own resonant frequency, but it is impractical to simultaneously obtain diverse power for selective loads with persistently high efficiency. It is worth mentioning that some literatures such as [19] and [20] put forward a time-sharing mechanism for power distribution of multiple loads in the single-frequency systems, essentially not transferring power simultaneously.

On the other hand, the multifrequency concept begins to be introduced into the multiload systems and is expected to find appropriate methods to supply energy with high efficiency and power distribution [21], [22]. Multiple transmitting coils are adopted and operated under respective arranged frequencies to simultaneously provide multifrequency power components for individual loads, as presented in [23] and [24]. In [23], all coils of transmitters and receivers are tuned into resonance at one common frequency, and the dynamic power distribution to selective loads and system efficiency can be enhanced by rotating a repeater that combines multifrequency power from transmitters and delivers power to receivers through couplings. In [24], the operating frequencies are widely apart and each pair of transmitting and receiving coils is tuned to a designed operating frequency, which means that traditional single-frequency theory can be utilized to handle the efficiency and power distribution issues. However, in [23] and [24], all the systems are composed of multiple transmitters, which will make the driver circuit configuration and transmitting coils complicated.

In this paper, a novel multifrequency circuit configuration for the MCR WPT system with multiple loads is proposed from a new perspective, in which a single transmitting resonant tank is driven simultaneously by multiple inverters sharing a common dc voltage source. As a representative example, the transmission characteristics of a double-frequency system with two loads are analyzed in detail based on the equivalent circuit model. Then, a methodology is proposed to explain the principle of achieving high efficiency and expected targeted power distribution. A superior feature of the proposed configuration and methodology is that the multifrequency power components from multiple inverters can be simultaneously delivered to multiple loads through a single transmitter. Meanwhile, the receiving coils are elaborately designed at different resonant frequencies that correspond to the operating frequencies of multiple inverters to achieve targeted power transfer and high efficiency, and the resonant frequencies of the transmitter and receivers are modulated to distribute power to selective loads. Finally, a prototype based on the proposed circuit configuration is built to confirm the validity of the methodology. As a comparison, an improved circuit configuration is presented for the double-load application and the system efficiency is increased by about 5%.

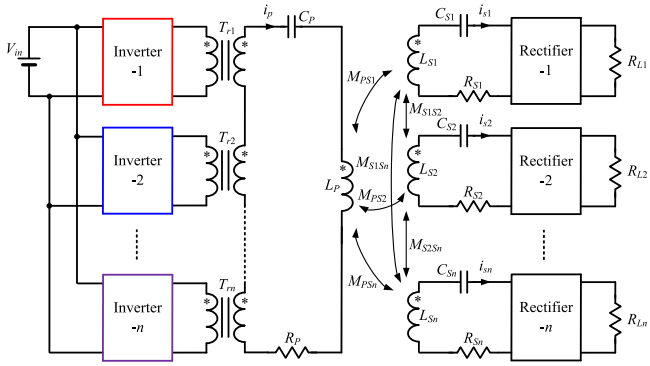


Fig. 1. Configuration of the multifrequency MCR WPT system with multiple loads.

## II. Description of the Proposed Multifrequency MCR WPT System With Multiple Loads

Fig. 1 shows the proposed circuit configuration of the multifrequency MCR WPT system with multiple loads. As illustrated, the transmitting resonant tank is driven by multiple voltage-fed inverters sharing a common dc voltage source and operating at multiple switching frequencies, namely $f_1, f_2, \ldots, f_n$. To combine the square voltages of each inverter under multiple frequencies, a superposition scheme that adopts secondary series-connected transformers is proposed, representing that the transmitting resonant tank is driven by a mixed-frequency square voltage. Multiple receivers cascaded by rectifiers are designed at different resonant frequencies that correspond to the respective switching frequencies, and the power components under different frequencies coming from the transmitter are expected to be transferred to the selective loads through the exclusive channel of specific frequency.

In Fig. 1, $L_P$ is the self-inductance of the transmitter including the leakage inductances of transformers. $L_{S1}, L_{S2}, \ldots, L_{Sn}$ are the self-inductances of receivers. $C_P, C_{S1}, C_{S2}, \ldots, C_{Sn}$ are the compensated capacitors. $R_P, R_{S1}, R_{S2}, \ldots, R_{Sn}$ are the equivalent series resistances and considered to be constant for simplicity, representing the conduction loss of coils, transformers, power semiconductors, etc. $M_{PSi}$ and $M_{SiSj}$ $(i = 1, 2, \ldots, n, j = 1, 2, \ldots, n, i < j)$ are the mutual inductances between transmitter and receivers.

In this paper, a typical double-frequency MCR WPT system with two loads is investigated in detail as a representative example for simplifying the theoretical analysis, and its circuit configuration is given in Fig. 2. As shown, two half-bridge inverters and double-voltage rectifiers are adopted for the voltage conversion, and external capacitors are inserted in series with the primary winding of transformers to block the output dc voltage component of inverters.

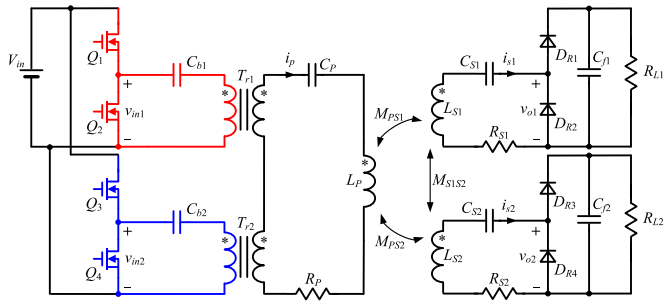


Fig. 2. Configuration of the double-frequency MCR WPT system with two loads.

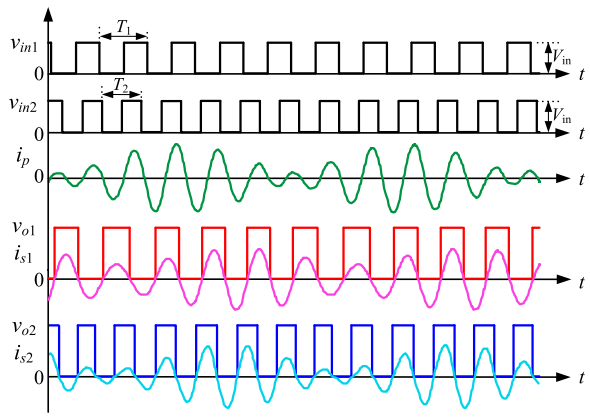


Fig. 3. Key voltage and current waveforms of the double-frequency MCR WPT system.

Fig. 3 depicts the key voltage and current waveforms of the double-frequency system. $v_{in1}$ and $v_{in2}$ are the midpoint voltages of half-bridge inverters operating at the frequencies of $f_1$ and $f_2$, respectively. $i_p, i_{s1}$, and $i_{s2}$ are the resonant currents of transmitting coils and receiving coils. $v_{o1}$ and $v_{o2}$ are midpoint voltages of double-voltage rectifiers. From Fig. 3, it can be known that the resonant currents consist of the multi-frequency components because the transmitting coils are driven by a mixed-frequency square voltage. Meanwhile, the dominant frequency components of each output are $f_1$ and $f_2$, which indicates that the power components at different frequencies are mainly transferred to the selective loads effectively.

## III. Modeling and Analysis of Transmission Characteristics

Generally, the quality factors of resonant tanks are high enough to adopt the fundamental harmonic analysis (FHA) method for the steady-state analysis, which only considers the fundamental component and neglects the dc component or higher harmonics. The equivalent circuit model of the system consisting of double-frequency components based on FHA is shown in Fig. 4, in which phasors $\dot{U}_{\rm in}^{(1)}$ and $\dot{U}_{\rm in}^{(2)}$, respectively, stand for the fundamental harmonics of the output ac voltages at frequencies of $f_1$ and $f_2$ in two half-bridge inverters with dc input voltage $V_{\rm in}$, phasors $\dot{I}_P^{(i)}$, $\dot{I}_{S1}^{(i)}$, and $\dot{I}_{S2}^{(i)}$ are the resonant currents of transmitter and receivers at $f_i$, respectively, and

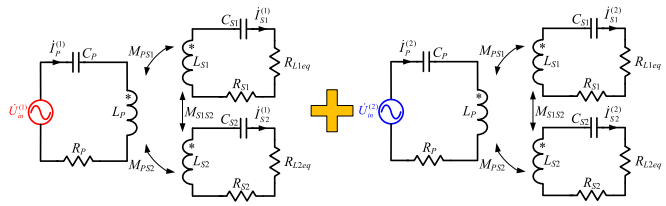


Fig. 4. Equivalent circuit model of the double-frequency MCR WPT system.

$R_{L1eq}$ and $R_{L2eq}$ are the equivalent values of load resistances $R_{L1}$ and $R_{L2}$ looking from the double-voltage rectifiers.

Due to the half-bridge configuration, the norms of $\dot{U}_{\rm in}^{(1)}$ and $\dot{U}_{\rm in}^{(2)}$ can be calculated as follows:

$$U_{\rm in}^{(1)} = \left\|\dot{U}_{\rm in}^{(1)}\right\| = \frac{\sqrt{2}}{\pi}V_{\rm in}, \quad U_{\rm in}^{(2)} = \left\|\dot{U}_{\rm in}^{(2)}\right\| = \frac{\sqrt{2}}{\pi}V_{\rm in}. \tag{1}$$

The relationships between the equivalent load resistances $R_{L1eq}, R_{L2eq}$ and the real load resistances $R_{L1}, R_{L2}$ are

$$R_{L1\rm eq} = \frac{2}{\pi^2}R_{L1}, \quad R_{L2\rm eq} = \frac{2}{\pi^2}R_{L2}. \tag{2}$$

At the steady state, the circuit matrix is given below at a certain operating frequency $f_i$ ($i = 1$ or 2)

$$\begin{bmatrix}\dot{U}_{\rm in}^{(i)}\\0\\0\end{bmatrix} = \begin{bmatrix}Z_P^{(i)} & -j\omega_i M_{PS1} & -j\omega_i M_{PS2}\\ -j\omega_i M_{PS1} & Z_{S1}^{(i)} & j\omega_i M_{S1S2}\\ -j\omega_i M_{PS2} & j\omega_i M_{S1S2} & Z_{S2}^{(i)}\end{bmatrix}\cdot\begin{bmatrix}\dot{I}_P^{(i)}\\ \dot{I}_{S1}^{(i)}\\ \dot{I}_{S2}^{(i)}\end{bmatrix} \tag{3}$$

where $\omega_i = 2\pi f_i$, $Z_P^{(i)} = R_P + j(\omega_i L_P - 1/\omega_i C_P)$, $Z_{S1}^{(i)} = R_{S1} + R_{L1\rm eq} + j(\omega_i L_{S1} - 1/\omega_i C_{S1})$, and $Z_{S2}^{(i)} = R_{S2} + R_{L2\rm eq} + j(\omega_i L_{S2} - 1/\omega_i C_{S2})$.

Solving (3), one can get

$$\dot{I}_P^{(i)} = \dot{U}_{\rm in}^{(i)} \Big/ Z_{\rm in}^{(i)} \tag{4}$$

$$\dot{I}_{S1}^{(i)} = \frac{\dot{U}_{\rm in}^{(i)}\left(\omega_i{}^2 M_{PS2}M_{S1S2} + j\omega_i M_{PS1}Z_{S2}^{(i)}\right)}{Z_{\rm in}^{(i)}\left[Z_{S1}^{(i)}Z_{S2}^{(i)} + (\omega_i M_{S1S2})^2\right]} \tag{5}$$

$$\dot{I}_{S2}^{(i)} = \frac{\dot{U}_{\rm in}^{(i)}(\omega_i{}^2 M_{PS1}M_{S1S2} + j\omega_i M_{PS2}Z_{S1}^{(i)})}{Z_{\rm in}^{(i)}\left[Z_{S1}^{(i)}Z_{S2}^{(i)} + (\omega_i M_{S1S2})^2\right]} \tag{6}$$

where the input impedance of the system is, Eqn. (7) as shown bottom of the next page.

Therefore, the transmission power of each load and the system efficiency at $f_i$ can be expressed as, Eqn. (8–10) as shown bottom of the next page, where Re() means the real part of a complex number.

As the two equivalent voltage sources of $f_1$ and $f_2$ drive the transmitter simultaneously, the total transmission power and the overall system efficiency can be obtained as

$$P_{o1} = P_{o1}^{(1)} + P_{o1}^{(2)} \tag{11}$$

$$P_{o2} = P_{o2}^{(1)} + P_{o2}^{(2)} \tag{12}$$

$$\eta_{\rm sys} = \frac{P_{o1}^{(1)} + P_{o1}^{(2)} + P_{o2}^{(1)} + P_{o2}^{(2)}}{P_{\rm in}^{(1)} + P_{\rm in}^{(2)}}. \tag{13}$$

According to the theoretical analysis above, it can be revealed that the transmission characteristics of the system are intensively related to the operating frequencies, the resonant frequency of transmitting tank, and the resonant frequencies of receiving tanks.

## IV. Methodology for High Efficiency and Targeted Power Distribution

For single-frequency MCR WPT systems, it is easy to achieve high system efficiency when the power distribution of multiple loads is irrespective. However, when specific demands of power allocation are taken into consideration, it will be difficult to realize high efficiency because the regulation of the mutual inductance and equivalent load resistances, as effective means of power distribution, makes the system efficiency very low at some operation points. In this paper, considering the transmission characteristics of the multifrequency system as analyzed above, a practical methodology for high efficiency and targeted power distribution of the multifrequency MCR WPT system is proposed in the following.

### A. Design for High System Efficiency

Substituting (10) into (13), the overall system efficiency can be expressed as

$$\eta_{\text{sys}} = k_1\eta_{\text{sys}}^{(1)} + k_2\eta_{\text{sys}}^{(2)} \tag{14}$$

where $k_1$ and $k_2$ are coefficients related to input power of the system, and $k_1 + k_2 = 1 (k_1 > 0$ and $k_2 > 0)$

$$k_1 = \frac{P_{\text{in}}^{(1)}}{P_{\text{in}}^{(1)} + P_{\text{in}}^{(2)}}, \quad k_2 = \frac{P_{\text{in}}^{(2)}}{P_{\text{in}}^{(1)} + P_{\text{in}}^{(2)}}. \tag{15}$$

From (14), $\eta_{\text{sys}}$ is the weighted average of $\eta_{\text{sys}}^{(1)}$ and $\eta_{\text{sys}}^{(2)}$. Obviously, high $\eta_{\text{sys}}$ can be easily realized if both $\eta_{\text{sys}}^{(1)}$ and $\eta_{\text{sys}}^{(2)}$ reach high values, respectively, and then the influence on the overall efficiency from the variations of $k_1$ and $k_2$ can be neglected.

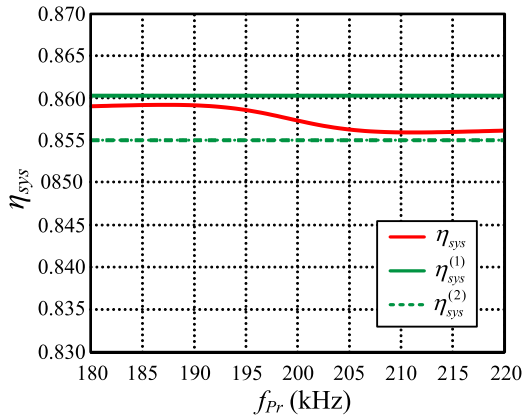


Fig. 5. System efficiency versus resonant frequency of the transmitter.

Under given specifications, as (10) revealed, $\eta_{\text{sys}}^{(i)}$ is principally influenced by operating frequency $f_i$ and resonant frequencies of receivers. To achieve high efficiency at both $f_1$ and $f_2$, the resonant frequency of Receiver 1 (corresponding to $R_{L1}$) $f_{S1r}$ is designed at $f_1$ and the resonant frequency of Receiver 2 (corresponding to $R_{L2}$) $f_{S2r}$ is tuned at $f_2$, i.e.

$$f_1 = \frac{1}{2\pi\sqrt{L_{S1}C_{S1}}}, f_2 = \frac{1}{2\pi\sqrt{L_{S2}C_{S2}}}. \tag{16}$$

Substituting (16) into (10), it can be found that both $\eta_{\text{sys}}^{(1)}$ and $\eta_{\text{sys}}^{(2)}$ can reach high levels. Fig. 5 illustrates the curves of system efficiency as a function of transmitting resonant frequency, and the specifications are listed as follows: $V_{\text{in}} = 24$ V, $f_1 = f_{S1r} = 190$ kHz, $f_2 = f_{S2r} = 210$ kHz, $L_P = L_{S1} = L_{S2} = 21\ \mu$H, $M_{PS1} = M_{PS2} = 1.7\ \mu$H, $M_{S1S2} = 0.39\ \mu$H, $R_P = 0.25\ \Omega$, $R_{S1} = R_{S2} = 0.11\ \Omega$, and $R_{L1} = R_{L2} = 10\ \Omega$. As shown in Fig. 5, the values of $\eta_{\text{sys}}^{(1)}$ and $\eta_{\text{sys}}^{(2)}$ are not affected by the transmitting resonant frequency, which can also be proved by (10). However, the system efficiency, $\eta_{\text{sys}}$ shows a slight difference under different transmitting resonant frequency, because the variation of $f_{pr}$ will change the input impedance at specific receiving resonant frequency according to (7), and the

$$Z_{\text{in}}^{(i)} = \frac{\dot{U}_{\text{in}}^{(i)}}{\dot{I}_P^{(i)}} = Z_P^{(i)} + \frac{(\omega_i M_{PS1})^2 Z_{S2}^{(i)} + (\omega_i M_{PS2})^2 Z_{S1}^{(i)} - j2\omega_i{}^3 M_{PS1} M_{PS2} M_{S1S2}}{Z_{S1}^{(i)} Z_{S2}^{(i)} + (\omega_i M_{S1S2})^2}. \tag{7}$$

$$P_{o1}^{(i)} = \left|\dot{I}_{S1}^{(i)}\right|^2 R_{L1\text{eq}} = \left|\frac{U_{\text{in}}\left(\omega_i{}^2 M_{PS2} M_{S1S2} + j\omega_i M_{PS1} Z_{S2}^{(i)}\right)}{Z_{\text{in}}^{(i)}\left[Z_{S1}^{(i)} Z_{S2}^{(i)} + (\omega_i M_{S1S2})^2\right]}\right|^2 R_{L1\text{eq}} \tag{8}$$

$$P_{o2}^{(i)} = \left|\dot{I}_{S2}^{(i)}\right|^2 R_{L2\text{eq}} = \left|\frac{U_{\text{in}}\left(\omega_i{}^2 M_{PS1} M_{S1S2} + j\omega_i M_{PS2} Z_{S1}^{(i)}\right)}{Z_{\text{in}}^{(i)}\left[Z_{S1}^{(i)} Z_{S2}^{(i)} + (\omega_i M_{S1S2})^2\right]}\right|^2 R_{L2\text{eq}} \tag{9}$$

$$\eta_{\text{sys}}^{(i)} = \frac{P_{o1}^{(i)} + P_{o2}^{(i)}}{P_{\text{in}}^{(i)}} = \frac{\left|\frac{\omega_i{}^2 M_{PS2} M_{S1S2} + j\omega_i M_{PS1} Z_{S2}^{(i)}}{Z_{S1}^{(i)} Z_{S2}^{(i)} + (\omega_i M_{S1S2})^2}\right|^2 R_{L1\text{eq}} + \left|\frac{\omega_i{}^2 M_{PS1} M_{S1S2} + j\omega_i M_{PS2} Z_{S1}^{(i)}}{Z_{S1}^{(i)} Z_{S2}^{(i)} + (\omega_i M_{S1S2})^2}\right|^2 R_{L2\text{eq}}}{\text{Re}\left(Z_{\text{in}}^{(i)*}\right)} \tag{10}$$

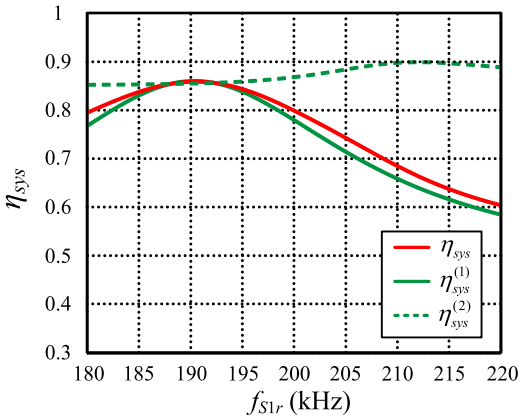


Fig. 6. System efficiency versus resonant frequency of Receiver 1.

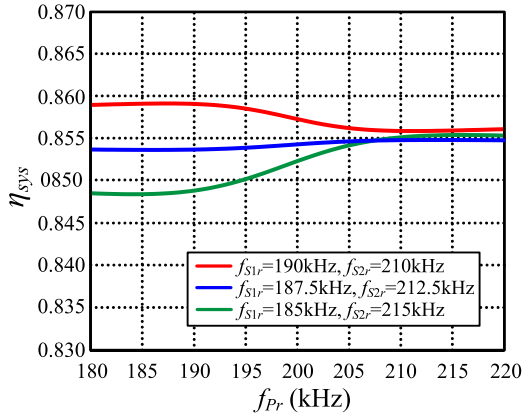


Fig. 7. Group of system efficiency under different transmitting and receiving resonant frequencies.

related input power will change accordingly. From (15), it can be known that $k_1$ and $k_2$ will change along with dynamically varied input power $P_{\text{in}}^{(1)}$ and $P_{\text{in}}^{(2)}$, which results in the variation of system efficiency tendency under different transmitting resonant frequency. It is noteworthy that the fluctuation of system efficiency curve is so minor that it can be neglected in the practical design. Due to $k_1 + k_2 = 1$ ($k_1 > 0$ and $k_2 > 0$), $\eta_{\text{sys}}$ always fluctuates between $\eta_{\text{sys}}^{(1)}$ and $\eta_{\text{sys}}^{(2)}$, and thus high overall system efficiency can be always achieved.

It should be noted that $\eta_{\text{sys}}^{(i)}$ ($i = 1$ or 2) is not the maximum value when $f_{S1r} = f_1$ and $f_{S2r} = f_2$. Assuming $f_{S2r} = f_2$, the system efficiency curves under various resonant frequencies of Receiver 1 is plotted in Fig. 6, in which $f_{Pr}$ is adopted at 200 kHz. Taking $\eta_{\text{sys}}^{(2)}$ as an example, as illustrated, $\eta_{\text{sys}}^{(2)}$ increases first and then decreases along with $f_{S1r}$. The peak value of $\eta_{\text{sys}}^{(2)}$ occurs in the vicinity of $f_2$ (210 kHz), instead of $f_1$ (190 kHz). However, if $f_{S1r}$ is tuned to the neighborhood of $f_2$ to maximize $\eta_{\text{sys}}^{(2)}$, the overall system efficiency $\eta_{\text{sys}}$ will dramatically decay along with $\eta_{\text{sys}}^{(1)}$, which indicates that the overall efficiency cannot be kept a high level only by maximizing $\eta_{\text{sys}}^{(2)}$. As a result, there is a tradeoff in designing $\eta_{\text{sys}}^{(1)}$ and $\eta_{\text{sys}}^{(2)}$, and each efficiency component should be taken into consideration comprehensively to obtain relatively high overall efficiency.

Given that the resonant frequencies of multiple receivers are severally tuned in accordance with the operating frequencies, a group of system efficiency curves with various receiving resonant frequencies as a function of transmitting resonant frequency is plotted in Fig. 7. As illustrated, the overall system efficiency can be generally maintained at a high level, and there is no obvious difference between efficiency curves under different groups of receiving resonant frequencies, which proves that the proposed high efficiency implementation method is insensitive to the variation of both receiving resonant frequencies and transmitting resonant frequency.

### *B. Method of Targeted Power Distribution*

Substituting (8), (9), and (16) into (11) and (12), the output power of $R_{L1}$ and $R_{L2}$ can be obtained, see (17) and (18) shown at the bottom of the next page.

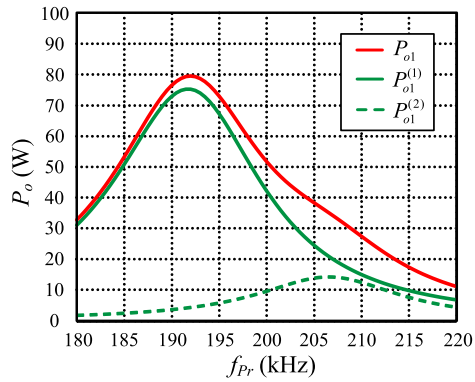


Fig. 8. Transmission power of Receiver 1 versus transmitting resonant frequency.

*1) Modulate the Resonant Frequency of the Transmitter:* From (17) and (18), the resonant frequency of the transmitter, $f_{Pr}$ is a key parameter that can be utilized for power distribution without detriment to the system efficiency. Through the modulation of $f_{Pr}$ within the adjacent area of $f_1$ and $f_2$, diverse targeted power distribution to the selective loads can be achieved.

For $R_{L1}$, as $f_{S1r}$ is designed at $f_1$ and differs from $f_2$, the impedance of Receiver 1 at $f_2$, $Z_{S1}^{(2)}$ is larger than that at $f_1$, $Z_{S1}^{(1)}$. The current component of $f_2$ $\dot{I}_{S1}^{(2)}$ is seriously attenuated compared to the component of $f_1$, $\dot{I}_{S1}^{(1)}$; thus, the power component of $f_2$ $P_{o1}^{(2)}$ is overall small and the majority of $P_{o1}$ is provided by the power component of $f_1$, $P_{o1}^{(1)}$, as shown in Fig. 8, which means that the variation trend of $P_{o1}$ is primarily determined by $P_{o1}^{(1)}$. And the peak value of $P_{o1}$ almost coincides with that of $P_{o1}^{(1)}$, by which the corresponding $f_{Pr}$ can be calculated by seeking for the minimum input impedance, $Z_{\text{in}}^{(1)}$. Similarly, the targeted power transfer to $R_{L2}$ can be obtained and the variation trend of $P_{o2}$ can be predicted through the modulation of $f_{Pr}$ under elaborative parameters design.

Comprehensively considering the double-frequency superposition on the two selective loads, the targeted power distribution as a function of transmitting resonant frequency is plotted in

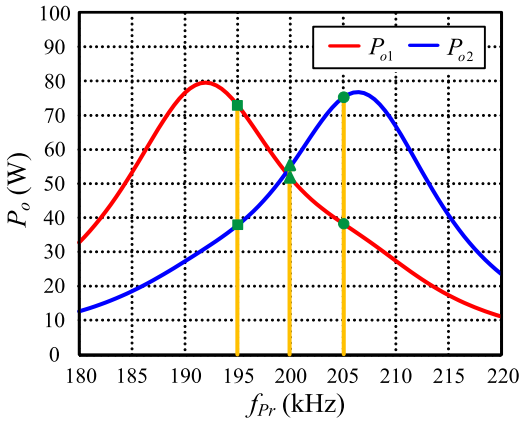


Fig. 9. Transmission power versus transmitting resonant frequency of two selective loads.

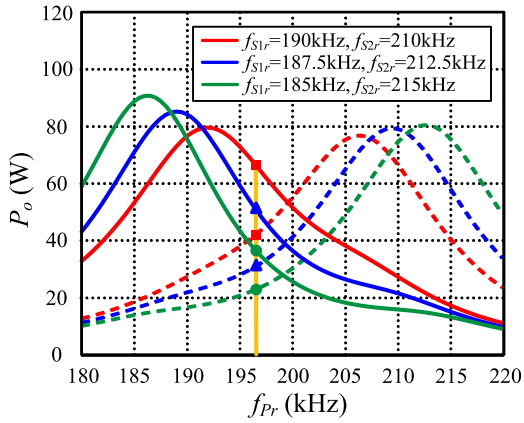


Fig. 10. Group of transmission power versus transmitting resonant frequency.

Fig. 9, in which three typical groups of power distribution are marked by solid lines with labels. As illustrated, varied power distribution is obtained successfully with wide range of power ratio by modulating $f_{Pr}$ elaborately.

*2) Modulate the Resonant Frequency of Receivers:* As an alternative, adjusting receiving resonant frequencies (equal to operating frequencies) can be treated as another effective means to implement the targeted power distribution. In Fig. 10, a group of transmission power curves versus transmitting resonant frequency is plotted under the aforementioned three series of receiving resonant frequencies, where $P_{o1}$ and $P_{o2}$ are illustrated in solid and dashed lines, respectively. As depicted, the peak transmission power of each load shifts along with various combinations of receiving resonant frequencies. By modulating receiving resonant frequencies, the power ratio of receivers can be controlled under a specific transmitting resonant frequency, as given by the solid line with different labels. It is noteworthy that two operating frequencies should be designed taking the transmitting resonant frequency into consideration together to achieve arbitrary targeted power distribution under the modulation of the resonant frequencies of transmitter and receivers.

$$P_{o1}=\left|\frac{U_{\text{in}}\left({\omega_1}^2 M_{PS2}M_{S1S2}+j\omega_1 M_{PS1}Z_{S2}^{(1)}\right)}{\left[Z_P^{(1)}+\dfrac{(\omega_1 M_{PS1})^2 Z_{S2}^{(1)}+(\omega_1 M_{PS2})^2 Z_{S1}^{(1)}-j2{\omega_1}^3 M_{PS1}M_{PS2}M_{S1S2}}{Z_{S1}^{(1)}Z_{S2}^{(1)}+(\omega_1 M_{S1S2})^2}\right]\left[Z_{S1}^{(1)}Z_{S2}^{(1)}+(\omega_1 M_{S1S2})^2\right]}\right|^2 R_{L1\text{eq}}$$
$$+\left|\frac{U_{\text{in}}\left({\omega_2}^2 M_{PS2}M_{S1S2}+j\omega_2 M_{PS1}Z_{S2}^{(2)}\right)}{\left[Z_P^{(2)}+\dfrac{(\omega_2 M_{PS1})^2 Z_{S2}^{(2)}+(\omega_2 M_{PS2})^2 Z_{S1}^{(2)}-j2{\omega_2}^3 M_{PS1}M_{PS2}M_{S1S2}}{Z_{S1}^{(2)}Z_{S2}^{(2)}+(\omega_2 M_{S1S2})^2}\right]\left[Z_{S1}^{(2)}Z_{S2}^{(2)}+(\omega_2 M_{S1S2})^2\right]}\right|^2 R_{L1\text{eq}} \tag{17}$$

$$P_{o2}=\left|\frac{U_{\text{in}}\left({\omega_1}^2 M_{PS1}M_{S1S2}+j\omega_1 M_{PS2}Z_{S1}^{(1)}\right)}{\left[Z_P^{(1)}+\dfrac{(\omega_1 M_{PS1})^2 Z_{S2}^{(1)}+(\omega_1 M_{PS2})^2 Z_{S1}^{(1)}-j2{\omega_1}^3 M_{PS1}M_{PS2}M_{S1S2}}{Z_{S1}^{(1)}Z_{S2}^{(1)}+(\omega_1 M_{S1S2})^2}\right]\left[Z_{S1}^{(1)}Z_{S2}^{(1)}+(\omega_1 M_{S1S2})^2\right]}\right|^2 R_{L2\text{eq}}$$
$$+\left|\frac{U_{\text{in}}\left({\omega_2}^2 M_{PS1}M_{S1S2}+j\omega_2 M_{PS2}Z_{S1}^{(2)}\right)}{\left[Z_P^{(2)}+\dfrac{(\omega_2 M_{PS1})^2 Z_{S2}^{(2)}+(\omega_2 M_{PS2})^2 Z_{S1}^{(2)}-j2{\omega_2}^3 M_{PS1}M_{PS2}M_{S1S2}}{Z_{S1}^{(2)}Z_{S2}^{(2)}+(\omega_2 M_{S1S2})^2}\right]\left[Z_{S1}^{(2)}Z_{S2}^{(2)}+(\omega_2 M_{S1S2})^2\right]}\right|^2 R_{L2\text{eq}} \tag{18}$$

where $Z_{S1}^{(1)}=R_{S1}+R_{L1\text{eq}}$, and $Z_{S2}^{(2)}=R_{S2}+R_{L2\text{eq}}$

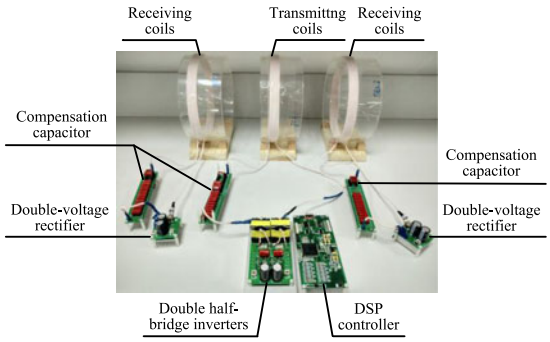


Fig. 11. Prototype of the proposed double-frequency system with two loads.

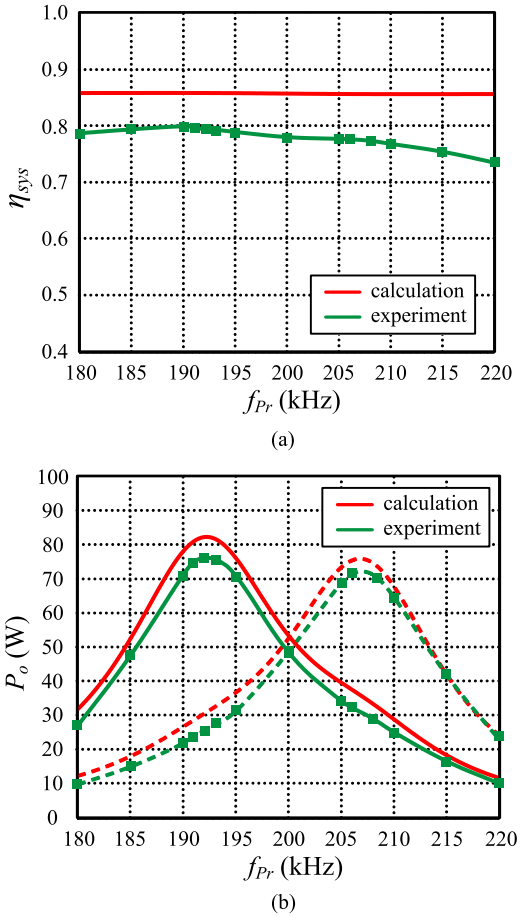


Fig. 12. Calculations and experiments of transmission characteristics when $f_1 = 190$ kHz and $f_2 = 210$ kHz based on original circuit configuration. (a) System efficiency. (b) Transmission power.

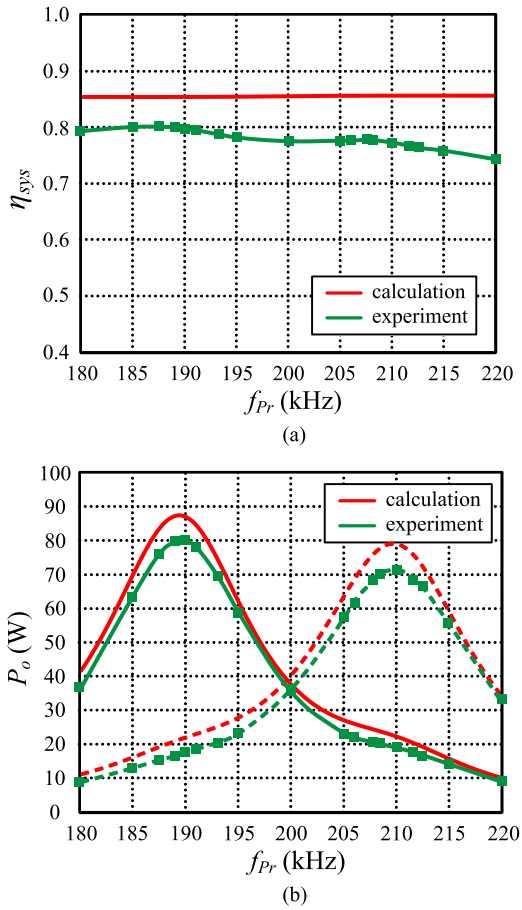


Fig. 13. Calculations and experiments of transmission characteristics when $f_1 = 187.5$ kHz and $f_2 = 212.5$ kHz based on original circuit configuration. (a) System efficiency. (b) Transmission power.

TABLE I
COMPARISONS BETWEEN DIFFERENT MULTILOAD/MULTIFREQUENCY WPT TOPOLOGIES

| | Transmission mechanism | Number of transmitting coils | System efficiency | System configuration |
|---|---|---|---|---|
| [18] | Simultaneous | Single | Medium | Simple |
| [19] | Time-sharing | Single | – | Simple |
| [23] | Simultaneous | Multiple | Medium | Complex |
| Proposed method in this paper | Simultaneous | Single | High | Simple |

### C. Comparison Between the Proposed Method and Other Multiload WPT Techniques

To illustrate the superior performance of the proposed superposition methodology in this paper, the comparison between different multiload and multifrequency MCR WPT topologies has been carried out in Table I, in the perspective of transmission mechanism, number of transmitters, system performance, etc. As shown in Table I, due to only one transmitting coil in the proposed configuration, the topology in this paper has a compact size and low weight; meanwhile, it can also achieve simultaneous power transfer to multiple loads and relatively high system efficiency by designing the resonant frequency of receivers appropriately.

## V. EXPERIMENTAL VERIFICATIONS

To verify the validity of the theoretical analysis and the feasibility of the proposed methodology, a prototype is implemented in the laboratory, as shown in Fig. 11. The specifications are given in Table II.

TABLE II
PARAMETERS OF THE PROTOTYPE

| Parameter | | Symbol | Value | Parameter | | Symbol | Value |
|---|---|---|---|---|---|---|---|
| Input voltage | | $V_{in}$ | 36V | Case 3 | Operating frequencies | $f_1$ | 185kHz |
| Inductance of transmitter | | $L_P$ | 22$\mu$H | | | $f_2$ | 215kHz |
| ESR of $L_P$ | | $R_P$ | 0.25Ω | | Capacitor of Receiver-1 | $C_{S1}$ | 34.89nF |
| Inductance of Receiver-1 | | $L_{S1}$ | 21.1$\mu$H | | Capacitor of Receiver-2 | $C_{S2}$ | 25.68nF |
| ESR of $L_{S1}$ | | $R_{S1}$ | 0.11Ω | Transmitting coil | Radius | $r_P$ | 11cm |
| Inductance of Receiver-2 | | $L_{S2}$ | 21.2$\mu$H | | Turns | $N_P$ | 7 |
| ESR of $L_{S2}$ | | $R_{S2}$ | 0.11Ω | Receiving coil-1 | Radius | $r_{S1}$ | 11cm |
| Load resistances | Receiver-1 | $R_{L1}$ | 10Ω | | Turns | $N_{S1}$ | 7 |
| | Receiver-2 | $R_{L2}$ | 10Ω | Receiving coil-2 | Radius | $r_{S2}$ | 11cm |
| Case 1 | Operating frequencies | $f_1$ | 190kHz | | Turns | $N_{S2}$ | 7 |
| | | $f_2$ | 210kHz | Transmission distance | Transmitter to Receiver-1 | $d_{PS1}$ | 15cm |
| | Capacitor of Receiver-1 | $C_{S1}$ | 33.15nF | | Transmitter to Receiver-2 | $d_{PS2}$ | 15cm |
| | Capacitor of Receiver-2 | $C_{S2}$ | 26.95nF | | Receiver-1 to Receiver-2 | $d_{S1S2}$ | 30cm |
| Case 2 | Operating frequencies | $f_1$ | 187.5kHz | Transformer ratio | | $N_{Trn}$ | 1:1 |
| | | $f_2$ | 212.5kHz | Mutual inductances | Transmitter to Receiver-1 | $M_{PS1}$ | 1.7$\mu$H |
| | Capacitor of Receiver-1 | $C_{S1}$ | 34.04nF | | Transmitter to Receiver-2 | $M_{PS2}$ | 1.7$\mu$H |
| | Capacitor of Receiver-2 | $C_{S2}$ | 26.43nF | | Receiver-1 to Receiver-2 | $M_{S1S2}$ | 0.39$\mu$H |

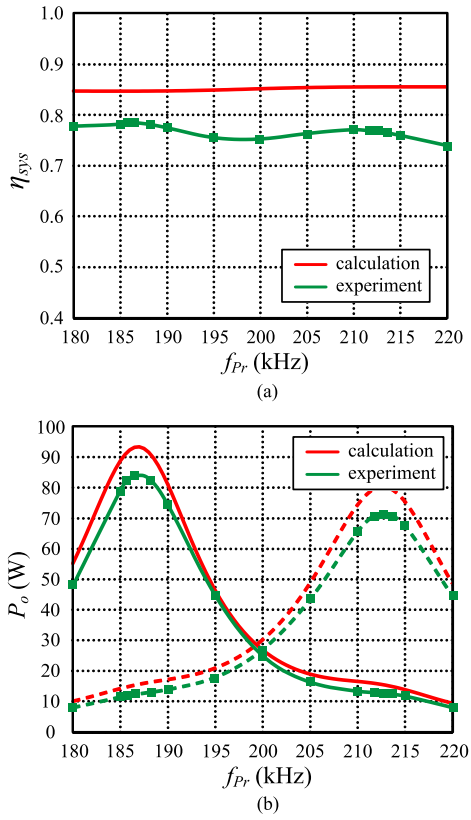


Fig. 14. Calculations and experiments of transmission characteristics when $f_1 = 185$ kHz and $f_2 = 215$ kHz based on original circuit configuration. (a) System efficiency. (b) Transmission power.

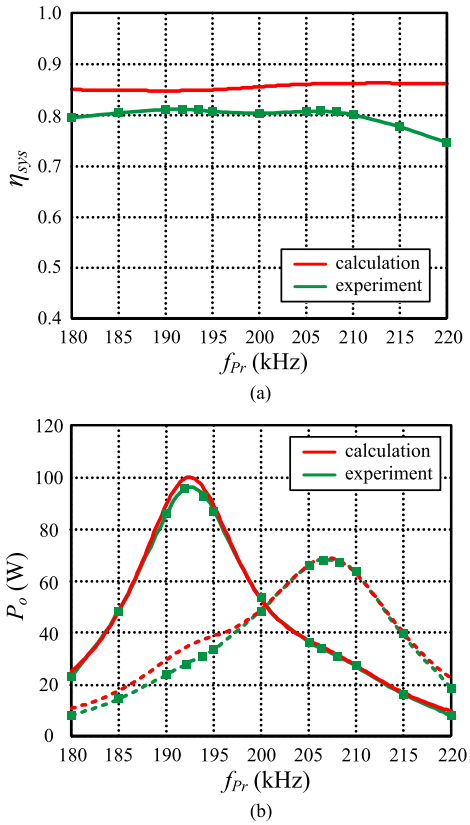


Fig. 15. Calculations and experiments of the system with unequal load ($R_{L1} = 15\ \Omega, R_{L2} = 10\ \Omega$) when $f_1 = 190$ kHz and $f_2 = 210$ kHz. (a) System efficiency. (b) Transmission power.

### A. Original Circuit Configuration

According to theoretical calculation and experimental measured data, the transmission characteristics with transmitting resonant frequency of $f_1 = 190$ kHz and $f_2 = 210$ kHz (Case 1) based on the original proposed circuit configuration in Fig. 2 are plotted in Fig. 12, and the other curves at $f_1 = 187.5$ kHz and $f_2 = 212.5$ kHz (Case 2), and $f_1 = 185$ kHz and $f_2 = 215$ kHz (Case 3) are shown in Figs. 13 and 14, respectively. It is observed that the experimental results are well in agreement with the the-

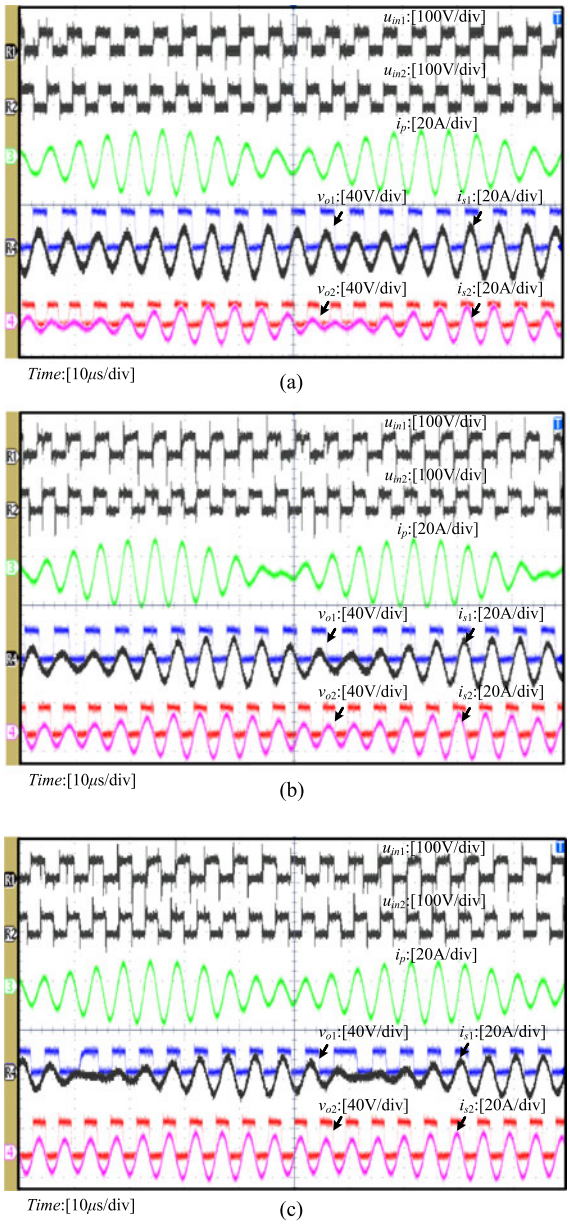


Fig. 16. Key experimental waveforms at $f_1 = 190$ kHz and $f_2 = 210$ kHz based on original circuit configuration. (a) $f_{Pr} = 190$ kHz. (b) $f_{Pr} = 200$ kHz. (c) $f_{Pr} = 210$ kHz.

oretical analysis by comparison. Thanks to the methodology of tuning the resonant frequencies of receivers at operating frequencies, high system efficiency can be always achieved within the variation of $f_{pr}$. There is a minor error between the theoretical and experimental efficiency due to the nonnegligible losses of power devices. And various power distributions of multiple loads are successfully realized simultaneously by the modulation of transmitting resonant frequency and receiving resonant frequencies.

As a necessary supplemental verification, Fig. 15 demonstrates the theoretical and experimental transmission characteristics of the system with unequal loads ($R_{L1} = 15\ \Omega, R_{L2} = 10\ \Omega$); as shown, the tendency of curves is similar to those of the system with equal load, and the output power of each

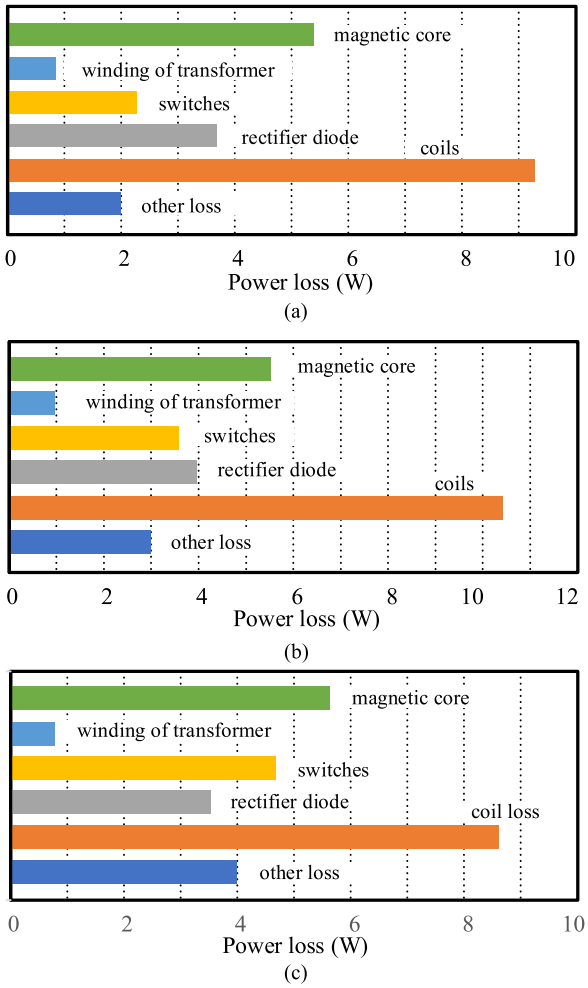


Fig. 17. Calculated power distribution when $f_1 = 190$ kHz and $f_2 = 210$ kHz. (a) $f_{Pr} = 190$ kHz. (b) $f_{Pr} = 200$ kHz. (c) $f_{Pr} = 210$ kHz.

load exists inherently a peak value in the adjacent area of resonant frequency point. Therefore, the proposed power distribution method is definitely applicable to the real system with independent and time-varying loads. In the real system, one can introduce a dc/dc converter cascaded at the output terminal of each rectifier to control the output power of each load; thus, the output power can be easily controlled independently by modulating the duty cycle of each dc/dc converter dynamically.

As an example, the key experimental waveforms at $f_1 = 190$ kHz and $f_2 = 210$ kHz under different transmitting resonant frequencies are given in Fig. 16. As shown, $i_{s1}$ and $i_{s2}$ mainly consist of two frequency components, which manifests that the output power of each load is inherently composed of the same frequency components. When $f_{Pr} = 190$ kHz, the midpoint voltage of Rectifier 1, $v_{o1}$ is larger than that of Rectifier 2, $v_{o2}$, which means that higher power is assigned to $R_{L1}$, and when $f_{Pr} = 210$ kHz, more power is distributed to $R_{L2}$. When $f_{Pr} = 200$ kHz, the output power of $R_{L1}$ and $R_{L2}$ is approximately equal as the output power curves overlap under this operation point according to Fig. 12.

Fig. 17 shows the calculated distribution of the power losses under the transmitting resonant frequency of 190, 200, and

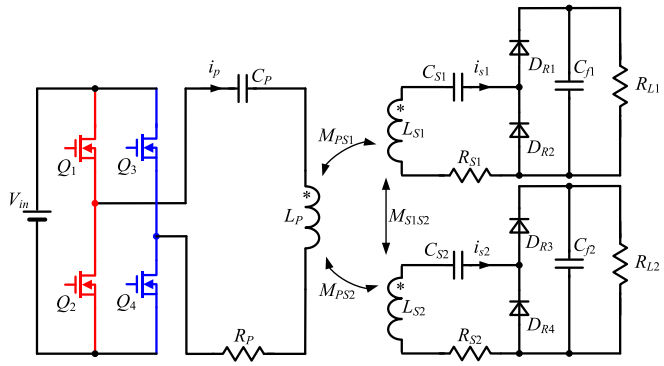


Fig. 18. Configuration of an improved double-frequency system with two loads.

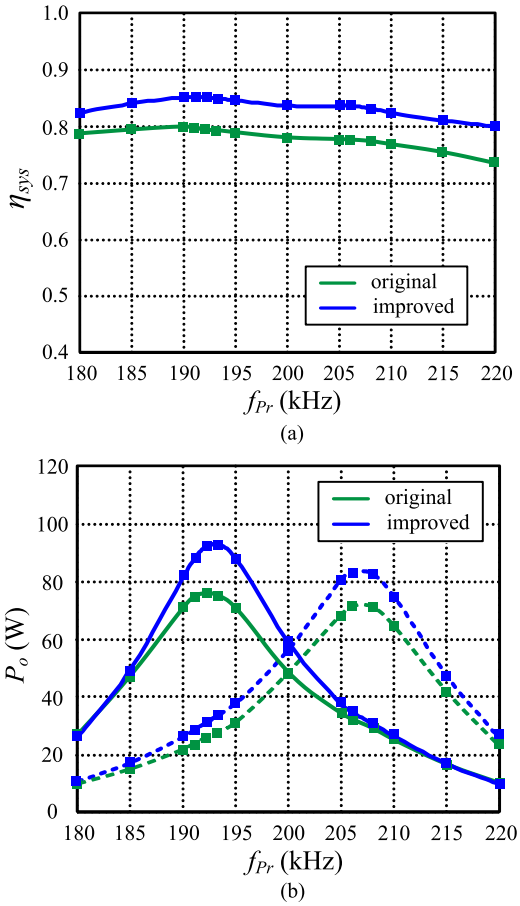


Fig. 19. Experimental transmission characteristics when $f_1 = 190$ kHz and $f_2 = 210$ kHz in the original and improved circuit configuration. (a) System efficiency. (b) Transmission power.

210 kHz. It can be observed that the power losses are dominantly distributed in transformers, transmitting coils, and receiving coils, in which the losses of transformers can be eliminated by removing the additional transformers. In double-load MCR WPT systems, the transformers can be easily saved by optimizing the driver circuit configuration, which will be discussed in the following. In multiload MCR WPT systems, the opportunities to get rid of the additional transformers really exist, such

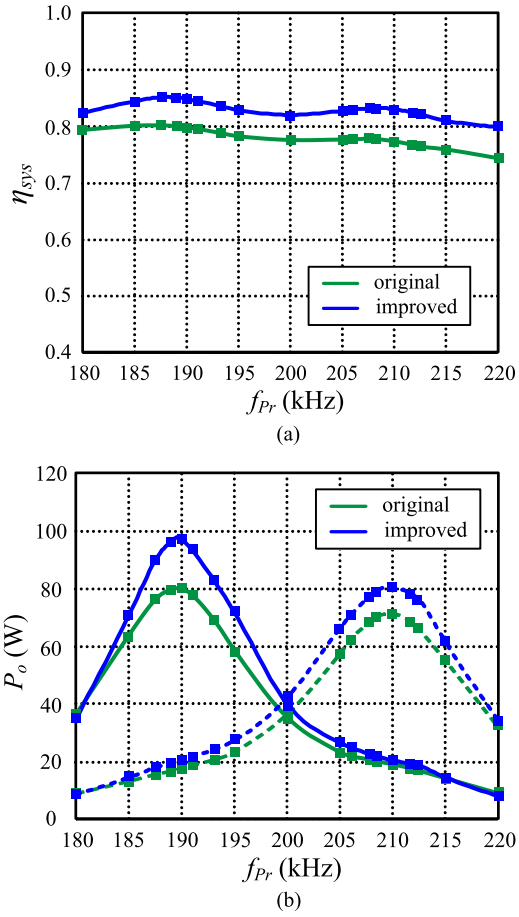


Fig. 20. Experimental transmission characteristics when $f_1 = 187.5$ kHz and $f_2 = 212.5$ kHz in the original and improved circuit configuration. (a) System efficiency. (b) Transmission power.

as integrating multiple driving signals with different switching frequency into power switches, which will be investigated thoroughly in the future work.

### B. Improved Circuit Configuration

Fig. 18 shows the improved double-frequency MCR WPT system without additional transformers, in which a full-bridge inverter is adopted and two bridge legs are operating at different switching frequencies. The output voltages of each bridge leg are subtracted to produce an alternative voltage driving the transmitting resonant tanks. Although this improved configuration cannot be extended to the application of multiple loads (more than two loads), it will be very beneficial to increase the overall efficiency for double-frequency and double-load MCR WPT system due to the removed transformers and dc blocking capacitors. Adopting same system parameters, the transmission characteristics versus transmitting resonant frequency of the original and improved topologies are plotted in Figs. 19–21. As shown, the system efficiency of improved circuit is increased by about 5% compared with the original driver circuit, owing to the reduction of the magnetic core loss and the transmitting equivalent resistance. Meanwhile, the overall power levels of each load are also improved.

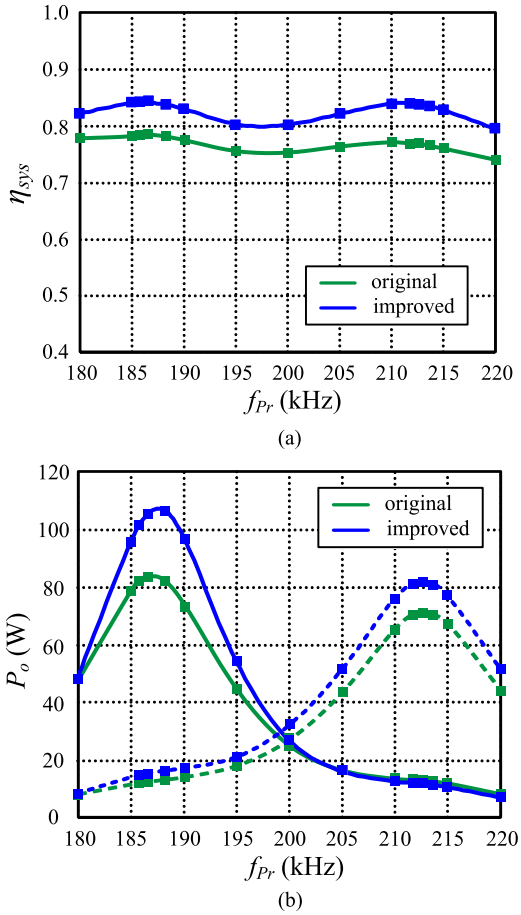


Fig. 21. Experimental transmission characteristics when $f_1 = 185$ kHz and $f_2 = 215$ kHz in the original and improved circuit configuration. (a) System efficiency. (b) Transmission power.

## VI. Conclusion

To provide energy for multiple loads with high system efficiency and targeted power distribution, the concept of multifrequency is proposed from a new perspective. A multifrequency driver circuit configuration for the MCR WPT system with multiple loads and an applicable superposition methodology are proposed in this paper. As a representative example, the transmission characteristics of a double-frequency system with two loads are analyzed, and the methodology is discussed in detail to explain the principle of achieving high efficiency and expected power distribution. The proposed configuration and methodology have the following superior characteristics: 1) the simultaneous multifrequency power transfer can be achieved by utilizing a mixed-frequency voltage superimposed by secondary series-connected transformers to drive a single transmitting tank; 2) the receiving coils are elaborately designed at different resonant frequencies that correspond to the operating frequencies of multiple inverters to achieve high system efficiency and make selective loads realize targeted power transfer; 3) through the modulation of the transmitting resonant frequency within the adjacent area of multiple operating frequencies, the power distribution to meet the requirements of selective loads can be realized; and 4) the resonant frequencies of receivers can also be modulated to effectively realize the power distribution. Moreover, an improved circuit configuration is put forward to increase the transmission efficiency in the application of the double-load MCR WPT system. Finally, experiments from two prototypes are implemented to verify the validity of the theoretical analysis and the feasibility of the proposed methodology.

## References

[1] F. Musavi, M. Edington, and W. Eberle, "Wireless power transfer: A survey of EV battery charging technologies," in *Proc. IEEE Energy Convers. Congr. Expo.*, 2012, pp. 1804–1810.

[2] H. Ramachandran and G. R. Bindu, "Wireless powering of utility equipments in a smart home using magnetic resonance," in *Proc. IEEE Recent Adv. Intell. Comput. Syst.*, 2013, pp. 221–226.

[3] S. Sugahara and S. Matsunaga, "Fundamental study of influence of ripple noise from DC–DC converter on spurious noise of wireless portable equipment," *IEEE Trans. Power Electron.*, vol. 31, no. 3, pp. 2111–2119, Mar. 2013.

[4] D. Ahn and S. Hong, "Wireless power transmission with self-regulated output voltage for biomedical implant," *IEEE Trans. Ind. Electron.*, vol. 61, no. 5, pp. 2225–2235, Oct. 2014.

[5] A. Kurs, A. Karalis, R. Moffatt, J. D. Joannopoulos, P. Fisher, and M. Soljacic, "Wireless power transfer via strongly coupled magnetic resonances," *Science*, vol. 317, no. 5834, pp. 83–86, Jul. 2007.

[6] N. Shinohara, "Power without wires," *IEEE Microw. Mag.*, vol. 12, no. 7, pp. S64–S73, Dec. 2011.

[7] M. G. Egan, D. L. O'Sullivan, J. G. Hayes, M. J. Willers, and C. P. Henze, "Power-factor-corrected single-stage inductive charger for electric vehicle batteries," *IEEE Trans. Ind. Electron.*, vol. 54, no. 2, pp. 1217–1226, Apr. 2007.

[8] X. Zhang and J. Chae, "Working distance comparison of inductive and electromagnetic couplings for wireless and passive underwater monitoring system of rinsing process in semiconductor facilities," *IEEE Sens. J.*, vol. 11, no. 11, pp. 2932–2939, May 2011.

[9] A. P. Sample, D. A. Meyer, and J. R. Smith, "Analysis, experimental results, and range adaptation of magnetically coupled resonators for wireless power transfer," *IEEE Trans. Ind. Electron.*, vol. 58, no. 2, pp. 544–554, Feb. 2011.

[10] F. Liu, Y. Yang, D. Jiang, X. Ruan, and X. Chen, "Modeling and optimization of magnetically coupled resonant wireless power transfer system with varying spatial scales," *IEEE Trans. Power Electron.*, vol. 32, no. 4, pp. 3240–3250, Apr. 2017.

[11] Y. Yang, F. Liu, and X. Chen, "A maximum power point tracking control scheme for magnetically coupled resonant wireless power transfer system by cascading SEPIC converter at the receiving side," in *Proc. IEEE Appl. Power Electron. Conf. Expo.*, 2017, pp. 3702–3707.

[12] H. Li, J. Li, W. Chen, and X. Yang, "A maximum efficiency point tracking control scheme for wireless power transfer systems using magnetic resonant coupling," *IEEE Trans. Power Electron.*, vol. 30, no. 7, pp. 3998–4008, Jul. 2015.

[13] J. Kim, H. C. Son, D. H. Kim, and Y. J. Park, "Impedance matching considering cross coupling for wireless power transfer to multiple receivers," in *Proc. IEEE Wireless Power Trans.*, 2013, pp. 226–229.

[14] Y. Zhang, T. Lu, Z. Zhao, F. He, K. Chen, and L. Yuan, "Employing load coils for multiple loads of resonant wireless power transfer," *IEEE Trans. Power Electron.*, vol. 30, no. 11, pp. 6174–6181, Nov. 2015.

[15] D. Ahn and S. Hong, "Effect of coupling between multiple transmitters or multiple receivers on wireless power transfer," *IEEE Trans. Ind. Electron.*, vol. 60, no. 7, pp. 2602–2613, Jul. 2013.

[16] H. Yin, M. Fu, C. Zhao, and C. Ma, "Power distribution of a multiple-receiver wireless power transfer system: A game theoretic approach," in *Proc. 41st Annu. Conf. IEEE Ind. Electron. Soc.*, 2015, pp. 1776–1781.

[17] M. Fu, T. Zhang, C. Ma, and X. Zhu, "Efficiency and optimal loads analysis for multiple-receiver wireless power transfer systems," *IEEE Trans. Microw. Theory Techn.*, vol. 63, no. 3, pp. 801–812, Mar. 2015.

[18] Y. Zhang, T. Lu, Z. Zhao, F. He, K. Chen, and L. Yuan, "Selective wireless power transfer to multiple loads using receivers of different resonant frequencies," *IEEE Trans. Power Electron.*, vol. 30, no. 11, pp. 6001–6005, Nov. 2015.

[19] Y. J. Kim, D. Ha, W. J. Chappell, and P. P. Irazoqui, "Selective wireless power transfer for smart power distribution in a miniature-sized multiple-receiver system," *IEEE Trans. Ind. Electron.*, vol. 63, no. 3, pp. 1853–1862, Mar. 2016.

[20] M. R. V. Moghadam and R. Zhang, "Multiuser wireless power transfer via magnetic resonant coupling: Performance analysis, charging control, and power region characterization," *IEEE Trans. Signal Inf. Process. Netw.*, vol. 2, no. 1, pp. 72–83, Mar. 2016.
[21] S. K. Papani, V. Neti, and B. K. Murthy, "Dual frequency inverter configuration for multiple-load induction cooking application," *IET Power Electron.*, vol. 8, no. 4, pp. 591–601, Apr. 2015.
[22] T. Hirokawa, E. Hiraki, T. Tanaka, M. Imai, K. Yasui, and S. Sumiyoshi, "Dual-frequency multiple-output resonant soft-switching inverter for induction heating cooking appliances," in *Proc. IEEE Annu. Conf. IEEE Ind. Electron. Soc.*, 2013, pp. 5028–5033.
[23] M. Q. Nguyen, Y. Chou, D. Plesa, S. Rao, and J. C. Chiao, "Multiple-inputs and multiple-outputs wireless power combining and delivering systems," *IEEE Trans. Power Electron.*, vol. 30, no. 11, pp. 6254–6263, Nov. 2015.
[24] C. Zhao and D. Costinett, "A dual-mode wireless power transfer system using multi-frequency programmed pulse width modulation," in *Proc. IEEE PELS Workshop Emerg. Technol. Wireless Power Trans.*, 2016, pp. 73–80.

**Fuxin Liu** (M'09–SM'16) was born in Heilongjiang Province, China, in 1979. He received the B.S., M.S., and Ph.D. degrees in electrical engineering from the Nanjing University of Aeronautics and Astronautics (NUAA), Nanjing, China, in 2001, 2004, and 2007, respectively.

In 2007, he joined the Faculty of the College of Automation Engineering, NUAA, where he is currently an Associate Professor. In 2017, he joined the Department of Electrical and Computer Engineering, Technical University of Munich (TUM), Munich, Germany, and served as a Visiting Professor. His main research interests include wireless power transfer, soft-switching dc/dc converters, and renewable energy generation systems.

Dr. Liu was awarded the August-Wilhelm Scheer Visiting Professorship of TUM, and serves as an Honorary Fellow of the TUM Institute for Advanced Study.

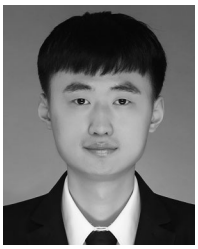

**Yong Yang** was born in Jiangsu Province, China, in 1993. He received the B.S. degree in electrical engineering and automation from the Nanjing University of Aeronautics and Astronautics, Nanjing, China, in 2015, where he is currently working toward the M.S. degree in electrical engineering.

His main research interests include wireless power transfer.

**Ze Ding** was born in Jiangsu Province, China, in 1996. He received the B.S. degree in electrical engineering and automation from the Nanjing University of Aeronautics and Astronautics, Nanjing, China, in 2017, where he is currently working toward the M.S. degree in electrical engineering.

His main research interests include wireless power transfer.

**Xuling Chen** (M'16) was born in Hunan Province, China, in 1979. She received the B.S., M.S., and Ph.D. degrees in mechanical and electrical engineering from the Nanjing University of Aeronautics and Astronautics (NUAA), Nanjing, China, in 2002, 2005, and 2011, respectively.

In 2005, he joined the Faculty of the College of Automation Engineering, NUAA, where she is currently a Lecturer. In 2017, she joined the Department of Electrical and Computer Engineering, Technical University of Munich, Munich, Germany, and served as a Visiting Scientist. Her main research interests include wireless power transfer, mechanical and electrical engineering, and mechanical design.

**Ralph M. Kennel** (M'89–SM'96) was born in Kaiserslautern, Germany, in 1955. He received the Diploma and Dr. Ing. (Ph.D.) degrees in electrical engineering from the University of Kaiserslautern, Kaiserslautern, in 1979 and 1984, respectively.

From 1983 to 1999, he worked on several positions with Robert BOSCH GmbH, Germany. Until 1997, he was responsible for the development of servo drives. From 1994 to 1999, he was a Visiting Professor with the University of Newcastle upon Tyne, Newcastle upon Tyne, U.K. From 1999 to 2008, he was a Professor of electrical machines and drives with Wuppertal University, Germany. Since 2008, he has been a Professor of electrical drive systems and power electronics with the Technical University of Munich, Munich, Germany. His current main research interests include renewable energy systems, sensorless control of ac drives, predictive control of power electronics, and hardware-in-the-loop systems.

Dr. Kennel is a Fellow of the IEE and a Chartered Engineer in the U.K. Within IEEE, he is a Treasurer of the Germany Section as well as ECCE Global Partnership Chair of the Power Electronics Society. He is an Associate Editor for the IEEE TRANSACTIONS ON POWER ELECTRONICS.